ADVANCED ENERGY MATERIALS
www.advenergymat.de

Highly Selective Conversion of CH_4 to High Value-Added C_1 Oxygenates over Pd Loaded ZnTi-LDH

Lei Fu, Ruixue Zhang, Jianlong Yang, Jiale Shi, Hai-Ying Jiang, and Junwang Tang**

The selective oxidation of methane to high value-added liquid oxygenated compounds under mild conditions is of great significance to promote the efficient utilization of the carbon source, but it also faces the dilemma of low activity and over-oxidation. Here, ZnTi-layered double hydroxides (LDH)-A200 photocatalysts with Pd loading are prepared to achieve efficient oxidation of methane, with O_2 as an oxidant under ambient condition. The highest generation rate of C_1 liquid products (methanol and formaldehyde) reaches 4924.47 μmol g^{-1} h^{-1} with a selectivity close to 100% over 0.5Pd-ZnTi-LDH-A200, which is 20 times higher than that of bare ZnTi-LDH-A200. The photochemical results show that the modified photocatalysts present much higher generation and separation efficiency of electron-hole pairs. In situ X–ray photoelectron spectroscopy indicates that Pd nanoparticles are the hole acceptor, which is beneficial to charge separation in the photocatalysis. Furthermore, electron spinresonance spectroscopy and temperature–programmed–desorption analysis prove that Pd loading is helpful to the adsorption of methane and oxygen on the surface of ZnTi-LDH-A200, promoting the production of reactive oxygen species and activation of methane. All these factors work together to promote the efficient conversion of CH_4 to high value-added C_1 oxygenates.

1. Introduction

As the main component of shale gas and combustible ice, methane is not only used as a common fuel, but also widely used to synthesize high value-added chemicals.[1–3] Traditionally, the industrial conversion of CH_4 generally through some indirect reforming methods, which are high-energy consumption due to the large C–H bond dissociation energy of CH_4.[4–6] Considering the increasingly serious energy problems nowadays, developing direct and energy-saved methods to convert CH_4 to high value-added chemicals is of great significance.[7–9] Limited by excessive oxidation, it is difficult to achieve both high conversion rate and high selectivity of CH_4 conversion at the same time.[10,11] Therefore, direct oxidation of CH_4 to high value-added chemicals still faces great challenges,[12,13] and it is necessary to develop new methods to realize both high conversion rate and high selectivity simultaneously under mild conditions.

By using the energy of sunlight, photocatalysis can activate inert molecules such as CH_4 under moderate conditions.[14,15] Theoretically, the excited photons can generate various reactive oxygen species (ROS), which also facilitates C–H dissociation of CH_4 molecules.[16–18] However, the photocatalytic activity for CH_4 conversion is very low because of the weak adsorption of CH_4 on the photocatalysts surface. With this consideration, layered double hydroxides (LDHs) attracted scientists' attention due to its distinctive 2D (2 dimensional) layered structure and large surface area, which may result in more active site exposure[19–23] and increase adsorption of small molecules.[24,25] As reported, LDHs have been widely used in photocatalytic ammonia synthesis and water splitting.[26–29] For example, the etched ZnCr-LDHs (ZnCr-1 h) was synthesized to be efficient for fixing N_2 and produce NH_3 at a rate of 33.19 μmol g^{-1} h^{-1} under ultraviolet and visible light radiation.[30] However, the efficiencies of LDHs are still very low in these reports because of the main disadvantages of low optical utilization and severe electron-hole pair recombination.[31,32] Hence, further improving the charge separation of LDHs to promote its performance is meaningful. Besides, increasing the adsorption of reactants by appropriate co-catalyst loading can also enhance the photocatalytic activities. Meanwhile, co-catalyst loading can promote the separation of photogenerated electrons and holes, which provides important guidance for the rational design of photocatalysts.[33–35]

L. Fu, R. Zhang, J. Yang, J. Shi, H.-Y. Jiang
Key Lab of Synthetic and Natural Functional Molecule Chemistry of Ministry of Education, the Energy and Catalysis Hub, College of Chemistry and Materials Science
Northwest University
Xi'an 710127, P. R. China
E-mail: jianghy@nwu.edu.cn

J. Tang
Department of Chemical Engineering
University College London
WC1E 7JE London, UK
E-mail: junwang.tang@ucl.ac.uk

The ORCID identification number(s) for the author(s) of this article can be found under https://doi.org/10.1002/aenm.202301118

DOI: 10.1002/aenm.202301118

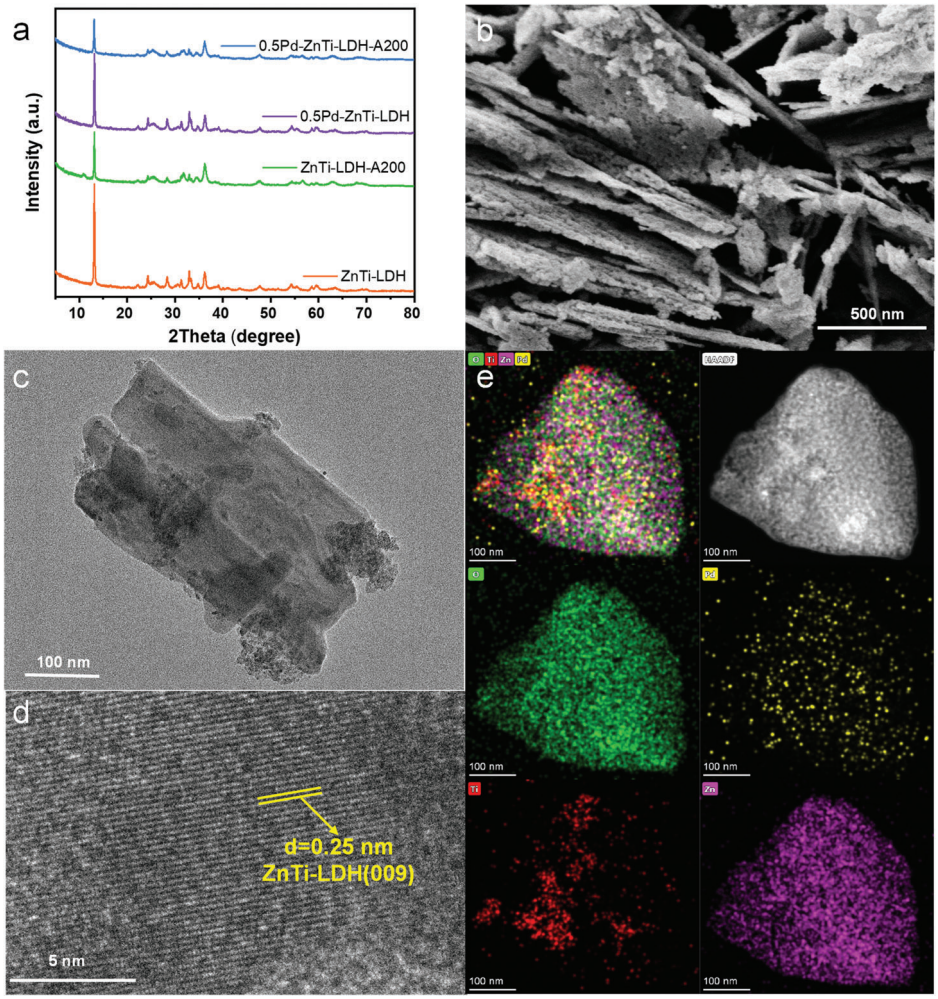

Figure 1. a) XRD patterns of the samples. b) SEM, c) TEM, d) HRTEM, and e) EDS-mapping images of 0.5Pd-ZnTi-LDH-A200. Green, red, yellow, and purple color represent O, Ti, Pd, and Zn elements, respectively.

In this work, the photocatalytic activity of ZnTi-LDH for CH_4 conversion to high value-added chemicals was investigated and its activity was further improved by Pd loading. Using O_2 as the oxidant in an aqueous solution, the highest yield of CH_4 conversion rate is achieved at 0.5Pd-ZnTi-LDH-A200, which is 4924.47 μmol g^{-1} h^{-1} with 100% selectivity to C_1 oxygenates, being 20 times higher than that of bare ZnTi-LDH-A200. The sample characterization and mechanism studies indicate that Pd loading significantly increases the light absorbance, as well as the generation and separation rates of photocarriers, which result in the improvement of photocatalytic generation of ROS. Besides, Pd loading also provides more exposed active sites for CH_4 and O_2 adsorption. All these factors synergistically improve the photocatalytic efficiency of ZnTi-LDH for CH_4 conversion.

2. Results and Discussion

2.1. Characterizations

The crystal structures of the prepared photocatalysts were analyzed by X-ray diffraction (XRD) patterns. The XRD spectra of ZnTi-LDHs are displayed in **Figure 1**a, which show similar diffraction patterns to the previous report.[36] The main diffraction peaks at $2\theta = 13.2°$ are attributed to (003) crystal plane of ZnTi-LDH, while the other peaks at 24.3°, 28.3°, 32.9°, and 36.2° are assigned to (006), (012), (101), and (009) crystal planes, respectively. After being calcined at low temperature of 200 °C, the XRD pattern of LDH are well maintained with the reduced peak intensity of $2\theta = 13.2°$, which may be caused by the partial collapse of the crystal lattice along with the loss of some inter-layer small molecules.[36] By loading Pd on the ZnTi-LDHs with and without calcination, no new diffraction peaks appeared, indicating the low amount and good dispersion of Pd nanoparticles on the surface of ZnTi-LDH (Figure 1a). 2D-layered structure of ZnTi-LDH was observed by scanning electron microscope (SEM) image in Figure 1b and N_2 adsorption-desorption isotherms in Figure S1, Supporting Information. It can be seen that all the modified and unmodified samples show typical IV isotherms and H3-type hysteresis loops ($P/P_0 > 0.4$), indicating the mesoporous structures with slit like pores comprised of aggregates (loose assemblages) of platelike particles.[37] The specific surface area (S_{BET}) was calculated by Brunauer–Emmett–Teller (BET) equation. The S_{BET} of

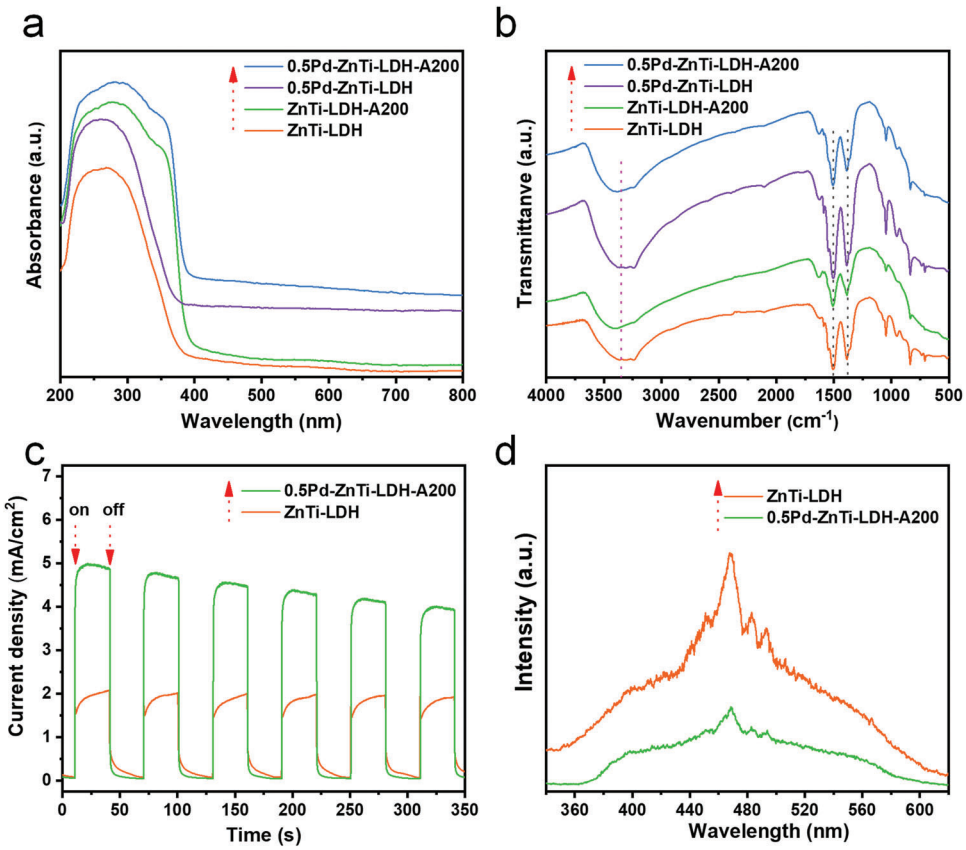

Figure 2. a) UV–vis diffuse reflectance;(b) FT-IR spectra of ZnTi-LDH, ZnTi-LDH-A200, 0.5Pd-ZnTi-LDH, and 0.5Pd-ZnTi-LDH-A200; c) Photocurrent responses and d) steady state fluorescence spectra of ZnTi-LDH and 0.5Pd-ZnTi-LDH-A200.

ZnTi-LDH, ZnTi-LDH-A200, 0.5Pd-ZnTi-LDH, and 0.5Pd-ZnTi-LDH-A200 are 89.8, 97.7, 84.0, and 87.7 $m^2\ g^{-1}$, and there is no significant differences, indicating that it's not the main factor to improve the catalytic performance of CH_4 transformation.[38] From Figure S2, Supporting Information, we can see that all ZnTi-LDHs samples retain the nanosheet structure with the size of about 300–500 nm.[31] Enlarging the transmission electron microscope (TEM) image of 0.5Pd-ZnTi-LDH-A200 in Figure 1c, the lattice fringes with $d = 0.25$ nm belong to the (009) crystal plane of LDHs can be clearly characterized by high-resolution transmission electron microscope (HRTEM) in Figure 1d. In addition, the elemental distribution of 0.5Pd-ZnTi-LDH-A200 was also analyzed by energy-dispersive spectroscopy mapping (EDS-mapping) to indicate the uniform dispersion of Pd on the surface of ZnTi-LDH (Figure 1e).[39]

The light absorption properties of the photocatalysts were studied by UV–vis diffuse reflectance spectra (UV-DRS), which is displayed in **Figure 2**a. The superimposed increment of the absorption at the range of 400–800 nm suggested the defective introduction and Pd loading for the sample of 0.5Pd-ZnTi-LDH-A200. Besides, according to the Tauc-plot curves,[40] the absorption band edge of ZnTi-LDH also shows some red shifts by the modification of single calcination, Pd loading or both (Figure S3, Supporting Information). Then, the prepared ZnTi-LDHs were characterized by Fourier transform infrared (FT-IR) spectra, which clearly shows that there are no obvious differences between the spectra of unmodified and modified ZnTi-LDH (Figure 2b), meaning that the modification processes did not change the structure of ZnTi-LDH. The broad peaks at 3200–3400 cm^{-1} are originated by the bonded and free O-H vibration on the surface of laminar layers,[41] while the peaks at 1505 and 1381 cm^{-1} are attributed to the vibrations of carbonate ions between the layers.[42] The element components of Pd-ZnTi-LDH-A200 were analyzed by X-ray photoelectron spectroscopy (XPS), and the results are displayed in Figure S4, Supporting Information. The binding energies of photoelectrons of Ti $2p_{1/2}$ and Ti $2p_{3/2}$ in Figure S4a, Supporting Information, are located at the binding energies of 464.1 and 458.5 eV with the interval of 5.6 eV, and no obvious peaks belong to Ti^{3+} are observed.[41] The binding energies of photoelectron of Zn $2p_{1/2}$ and Zn $2p_{3/2}$ in Figure S4b, Supporting Information, are located at 1044.4 and 1021.4 eV with the interval of 23.0 eV.[39] These results are in good agreement with previously reported values, indicating the successful preparation of ZnTi-LDH photocatalyst.

To further investigate the generation and separation of photo charge carriers, the photocurrent density and photoluminescence of the ZnTi-LDHs were performed. The positive photocurrent densities in Figure 2c mean that ZnTi-LDH is an n-type semiconductor. After modification, the photocurrent density of ZnTi-LDH was significantly improved, suggesting the increased generation of photocarriers. Meanwhile, the luminescence density of ZnTi-LDH was also remarkably depressed (Figure 2d),

indicating the efficient reduction of charge recombination. Moreover, the transient fluorescence spectra of ZnTi-LDHs were also tested and fitted in Figure S5, Supporting Information, where τ_1 and τ_2 are the decay times of the photocarriers, α_1 and α_2 are the corresponding coefficients. The fast decay component τ_1 represents the radiation emission generated by direct inter-band exciton recombination, and the slow decay component τ_2 involves the radiation emission originated by indirect recombination of excited electrons and valence band holes. It could be obviously founded from Table S1, Supporting Information, that both τ_1 and τ_2 of 0.5Pd-ZnTi-LDH-A200 (τ_1 = 1.18 ns, τ_2 = 6.19 ns) are slightly larger than those of ZnTi-LDH (τ_1 = 1.04 ns, τ_2 = 5.01 ns). The average lifetime of 0.5Pd-ZnTi-LDH-A200 (τ = 3.27 ns) calculated by $\tau = (\alpha_1{\tau_1}^2 + \alpha_2{\tau_2}^2)\cdot(\alpha_1\tau_1 + \alpha_2\tau_2)^{-1}$ is also longer than that of ZnTi-LDH (τ = 2.78 ns), suggesting more efficient separation of photocarriers by 0.5Pd-ZnTi-LDH-A200 than that by ZnTi-LDH.[43] The higher generation rate, lower recombination rate and longer lifetime of photocarriers over 0.5Pd-ZnTi-LDH-A200 proposes a potentially higher photocatalytic performance.

2.2. Photocatalytic CH_4 Conversion

The photocatalytic performance of Pd-ZnTi-LDHs-A200 was investigated by the conversion of CH_4 to C_1 oxygenates at ambient temperature and under 2.0 MPa pressure, with O_2 as the oxidant in water. In this work, the produced C_1 oxygenates with high added value from CH_4 conversion were detected by NMR and determined to be mainly CH_3OH and HCHO, while CO_2 was considered as the by-product of excessive oxidation. Specifically, $^{13}CH_4$ isotope labeling experiments were first performed to qualitatively confirm the liquid products. In ^{1}H-NMR spectrum of **Figure 3**a, the peak of chemical shift at 3.2 ppm is attributed to CH_3OH,[33] and that at 2.5 ppm is the internal standard DMSO.[34] The ^{13}C-NMR spectrum was acquired by using 0.4 MPa $^{13}CH_4$ as the reactant. The peaks in Figure 3b with the chemical shifts of 81.4 and 48.5 ppm are attributed to $^{13}CH_3OH$ and $HO^{13}CH_2OH$ (methylene diol, the main form of HCHO in aqueous solution), respectively.[44] The above NMR results not only determine that the liquid product of the reaction contains CH_3OH and HCHO, but also confirm the carbon source of liquid products is mainly derived from CH_4. Interestingly, the unstable product of CH_3OOH were not detected by NMR, different to our previous reports.[33,45] This may be because of the strong adsorption of ·OOH or CH_3OOH on the surface of Pd-ZnTi-LDH-A200, resulting in the fast reduction of them to ·OH or CH_3OH.[13,46,47]

The catalytic activities of the prepared photocatalysts were evaluated by quantitatively measuring the generation rates of C_1 oxygenate products. The generation of liquid products CH_3OH and gas product CO_2 were quantified by GC equipped with TCD and FID detectors, while the generation of HCHO was quantified by a colorimetric method[48] with a standard curve (Figure S6, Supporting Information). In Figure 3c, the original ZnTi-LDH without calcination and Pd loading shows very poor performance for CH_4 conversion with only a slow rate of HCHO production (299.95 μmol g^{-1} h^{-1}). It is widely reported that co-catalyst loading is beneficial to improve the activity of photocatalysts,[40,49] herein Pd was photo deposited on the surface of the prepared ZnTi-LDH. However, the activity improvement for C_1 products is very limited by Pd loading, which is only 1.8 times higher (557.13 μmol g^{-1} h^{-1}) than the unloaded ZnTi-LDH. This may be because that the hydroxyl group on the surface of ZnTi-LDH is not conducive to Pd loading,[38] so we calcined ZnTi-LDH at low temperature of 200 °C in order to partially remove the surface hydroxyl group, and named the calcined sample as ZnTi-LDH-A200. Comparatively, the CH_4 conversion activity of the calcined ZnTi-LDH is not significantly improved. Then, Pd nanoparticles were photo deposited on the surface of ZnTi-LDH-A200 and obtained a surprising C_1 oxygenates generation rate (4924.47 μmol g^{-1} h^{-1}) for CH_4 conversion, while tiny overoxidation production of CO_2 was produced (inset of Figure 3c). The experimental results in Figure 3d show a volcanic trend relationship between the loading amount of Pd and C_1 oxygenates production rate. The highest C_1 oxygenates generation rate is achieved at 0.5Pd-ZnTi-LDH-A200 with the selectivity of ≈100%, which is 20 times higher than that of bare ZnTi-LDH-A200. The C_1 oxygenates production rates of all the experiments are listed in Table S2, Supporting Information, as well as the control experiments.

Although other noble metal (Au, Ag, and Pt) loading can also improve the photocatalytic activity of ZnTi-LDH, there is still a big gap compared with Pd loading (Figure 3e). This may be because of different role of Pd for the photocatalytic activity enhancement. Here, Pd likely acts as the hole acceptor,[45,49] while Au, Ag and Pt act as electron acceptor,[50] which will be discussed later. Most importantly, the activity of used photocatalysts for highly selective CH_4 conversion can be recovered by simple calcination for 3 h at the temperature of 200 °C. About 85% of the activity is kept after 4 cycles' CH_4 conversion reaction. And it can be seen from Figure S7, Supporting Information, that the XRD pattern of the selected photocatalyst does not change significantly after CH_4 conversion reaction, while its micro-structure remains the same after the CH_4 conversion in Figure S8, Supporting Information, indicating its good stability during the photocatalytic CH_4 conversion reaction. Furthermore, the photocatalytic experiments of CH_4 conversion under the light with different wavelength of 365, 400, 420, and 450 nm were performed to study the relationship between the photocatalytic activity and light wavelength. The results in Figure S9, Supporting Information, indicate that the photocatalytic activity of the selected catalyst is strongly related to the wavelength of the light we used.

2.3. Mechanism Study

CH_4 temperature-programmed desorption (CH_4-TPD) experiments were carried out to evaluate the adsorption of CH_4 on the surface of different ZnTi-LDHs. Before TPD analysis, the TG spectrum were collected and shown in **Figure 4**a. The result represents that the layered structure of ZnTi-LDH would collapse[51] and metal oxide of TiO_2 and ZnO (Figure S10, Supporting Information) would appear when the calcination temperature is higher than 250 °C, which is consistent with the previous reports.[38,52] On this basis, the chemisorption of CH_4 is evaluated by the peak at 203 °C in Figure 4b. To investigate the effect of the calcination temperature to the activity, we compared the photocatalytic activities of ZnTi-LDH calcined at different temperatures. The results in Figure S11, Supporting Information

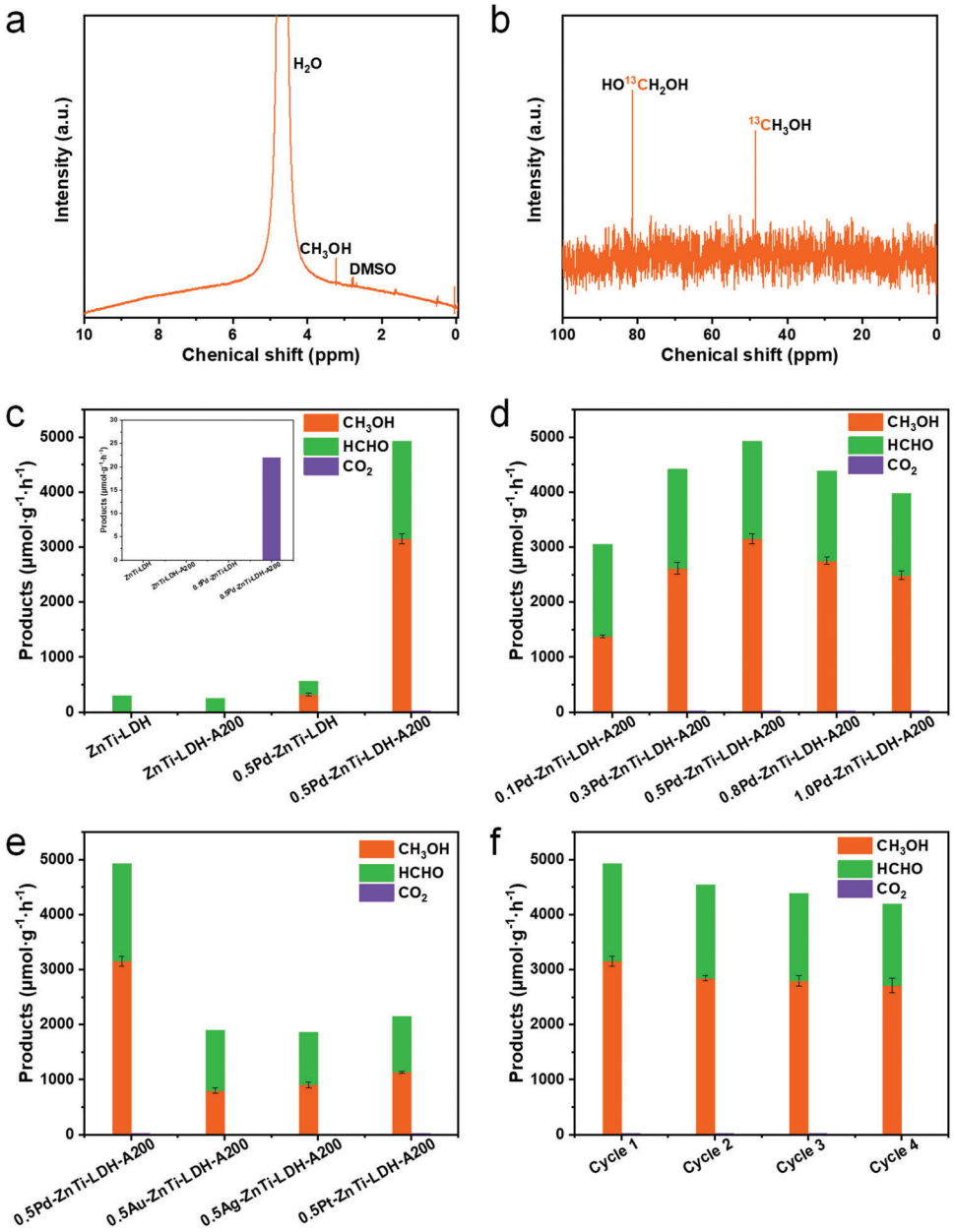

Figure 3. a) ^{1}H-NMR spectrum and b) ^{13}C-NMR spectrum of the liquid products of photocatalytic CH_4 conversion by ZnTi-LDHs. Photocatalytic production rate of C_1 oxygenates over c) different ZnTi-LDHs; d) Pd-ZnTi-LDH-A200 with different Pd loading amounts; e) ZnTi-LDH-A200 loaded by different noble metals. f) Cycling experimental results of 0.5Pd-ZnTi-LDH-A200. Standard reaction conditions: 20 mg photocatalyst, 100 mL distilled H_2O, 1.9 MPa CH_4, 0.1 MPa O_2, Xenon lamp illumination 2 h.

indicate that increasing the calcination temperature of ZnTi-LDH cannot improve the photocatalytic activity. However, the calcination of ZnTi-LDH is beneficial for the Pd loading (Figure S12, Supporting Information), which is demonstrated to be the main reason of the photocatalytic activity enhancement in Figure 3c,d. Obviously in Figure 4b, the loaded Pd on the surface of ZnTi-LDH provides some adsorption sites of CH_4 molecules, resulting in the enhanced CH_4 conversion rate. The charge transfer from ZnTi-LDH-A200 to Pd was observed by in situ XPS spectra in Figure 4c. In dark, the peaks at 343.61 and 338.29 eV are attributed to $3d_{32}$ and $3d_{52}$ orbits of Pd^{2+}.[53] Under full spectrum light irradiation, they shift to 343.74 and 338.52 eV, which confirm the hole acceptor role of Pd^{2+} in the photocatalytic processes by ZnTi-LDH-A200.[45] The TPD and XPS results demonstrate that Pd acts not only as the adsorption site of CH_4, but also as the hole acceptor of ZnTi-LDH-A200. In the EPR spectrum of 0.5Pd-ZnTi-LDH-A200 shown in Figure 4d, the signal peak at $g = 2.076$ is assigned to the adsorbed oxygen, indicating the efficient adsorption of O_2 molecules.[40,49] The signal peak at $g = 2.028$ is attributed to the oxygen radicals of O^{-} ($Ti^{4+}O^{2-}Ti^{4+}O^{-}$),[42,54,55]

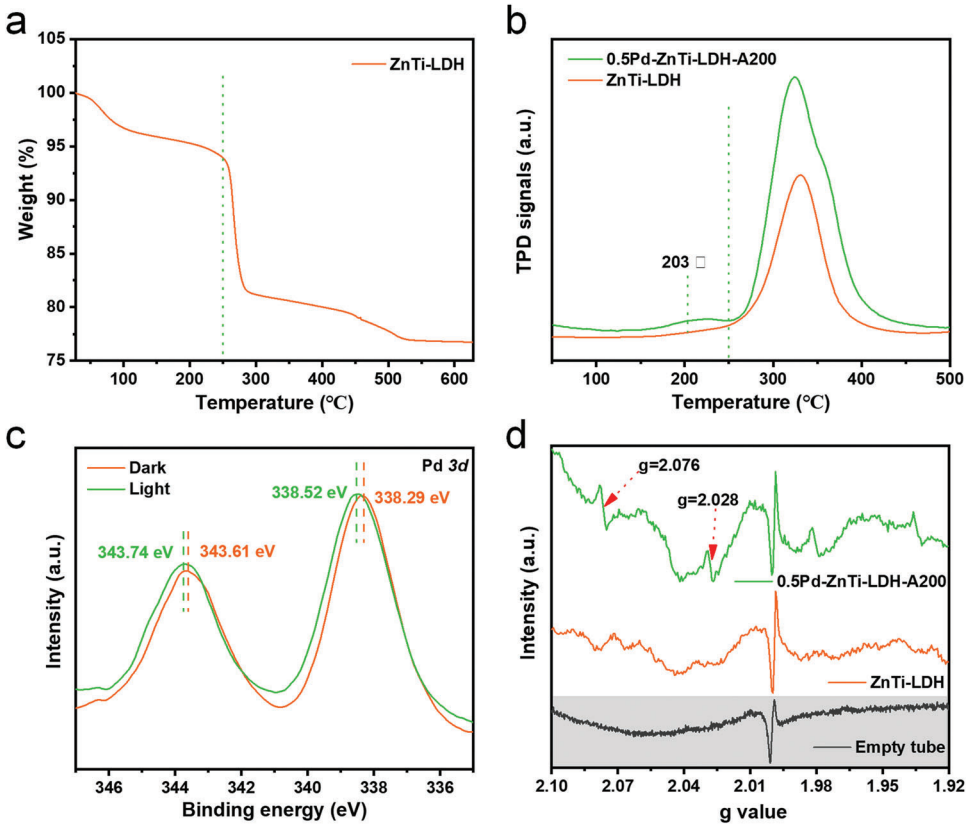

Figure 4. a) TG curves of ZnTi-LDH. b) CH_4-TPD spectra of ZnTi-LDH and 0.5Pd-ZnTi-LDH-A200. c) In situ Pd_{3d} XPS spectra of 0.5Pd-ZnTi-LDH-A200 in dark and under light irradiation. d) EPR spectra illustrating the trapped sites at −173 °C in the air: empty tube, ZnTi-LDH and 0.5Pd-ZnTi-LDH-A200.

which was reported to be formed by the trapping of photoproduced holes. ERP tests indicate that Pd loading is conductive to the adsorption of O_2 molecules on the defective site of ZnTi-LDH, which may result in the generation of more reactive oxygen species and enhanced CH_4 oxidation.

Considering the generation of reactive oxygen species (ROS, i.e., $O_2^{-\cdot}$ and ·OH), the band structure of ZnTi-LDH and 0.5Pd-ZnTi-LDH-A200 was characterized by Tauc plot curve and Mott–Schottky plot curve. The band gaps (E_g) of ZnTi-LDH and 0.5Pd-ZnTi-LDH-A200 are calculated to be 3.54 and 3.23 eV from Figure S3, Supporting Information. Their conduction band potentials are obtained by the flat band potentials measured by Mott-Schottky plot curves in Figure S13, Supporting Information. The positive slopes of the samples indicate that the catalysts are n-type semiconductors, for which the flat band potential is located about 0.2 eV below the conduction band (E_{CB}). Accordingly, their conduction band potentials (E_{CB}) are determined to be −0.63 and −0.74 V (versus NHE), and their valence band potentials (E_{VB}) are calculated to be 2.91 and 2.49 V (versus NHE), respectively. These results imply that the band potentials of ZnTi-LDH and 0.5Pd-ZnTi-LDH-A200 are theoretically sufficient to generate ROS of $O_2^{-\cdot}$ and ·OH.[56,57] Under full spectrum light irradiation, the surface adsorbed O_2 on 0.5Pd-ZnTi-LDH-A200 can be effectively reduced to $O_2^{-\cdot}$, which is further proved by in situ EPR study with DMPO as the radical trap in acetonitrile. As displayed in **Figure 5**a, no signal is detected in dark, while six distinct peaks (A_H = 9.4 G, A_N = 13.6 G) appear under light irradiation. The sextuple peaks are the characteristic peaks of DMPO-OOH,[58] indicating the formation of $O_2^{-\cdot}$ on the surface of 0.5Pd-ZnTi-LDH-A200 under light irradiation. What's more, the generation of $O_2^{-\cdot}$ were also quantitatively measured by NBT method.[56,59] According to the fitting results by first-order kinetics in Figure 5b, the k constant of 0.5Pd-ZnTi-LDH-A200 is determined to be 0.0354 min^{-1}, which is five times bigger than that of ZnTi-LDH (0.0065 min^{-1}). Subsequently, the generation of ·OH by 0.5Pd-ZnTi-LDH-A200 were also measured by in situ EPR study and CA method. The ERP experiments were carried out by using DMPO as the radical trap in water. Similarly, no peaks is observed before illumination, and a quadruplex peaks (A_H = 14.9 G, A_N = 14.9 G) with a relative intensity of 1:2:2:1, belong to DMPO-OH,[60,61] appear after illumination (Figure 5c). The generation of ·OH is represented by the PL intensity of generated 7-OH-CA by the reaction between ·OH and CA. The PL intensity of 7-OH-CA generated by 0.5Pd-ZnTi-LDH-A200 is significantly higher than that by ZnTi-LDH, suggesting much more ·OH generation (Figure 5d).

Furthermore, isotope labeling experiments were carried out to determine the oxygen source in the products of C_1 oxygenate. The experimental results show that $CH_3{}^{16}OH$ and its fragment peaks (m/z = 31, 32) were detected when $H_2{}^{18}O$ and $^{16}O_2$ were used (**Figure 6**a), while $CH_3{}^{18}OH$ and the fragment peaks (m/z = 33, 34) were detected when $H_2{}^{16}O$ and $^{18}O_2$ were used (Figure 6b).[45] These results prove that the oxygen of the C_1 oxygenate products mainly come from O_2, but not H_2O.

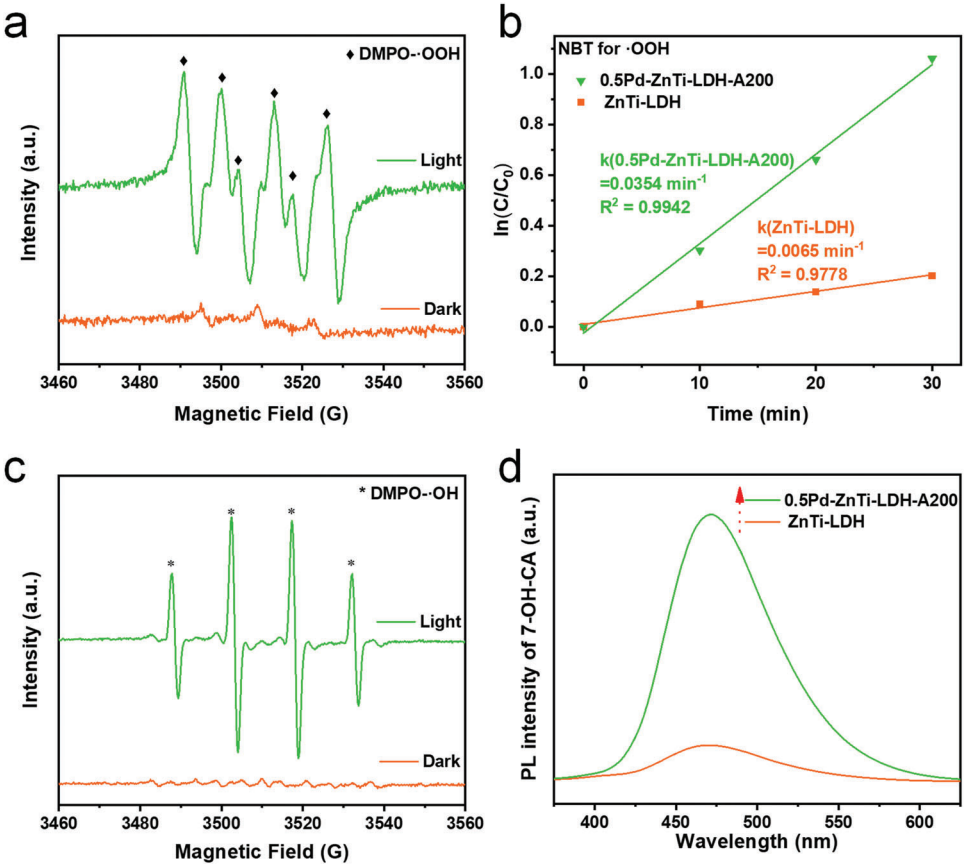

Figure 5. a) In situ EPR spectra of DMPO-OOH over 0.5Pd-ZnTi-LDH-A200 in acetonitrile solution. b) First-order kinetic constant of NBT photodegradation reaction for detection of ·OOH radical formation. c) In situ EPR spectra of DMPO-OH over 0.5Pd-ZnTi-LDH-A200 in water. d) PL spectra of the 7-OH–CA for ·OH radical measurement over different photocatalysts.

Based on the results and discussions above, the photocatalytic mechanism of selective oxidation of CH_4 on 0.5Pd-ZnTi-LDH-A200 is proposed in **Scheme 1**.[62] Under light illumination, electrons on the valence band of ZnTi-LDH-A200 are excited to the conduction band, forming the holes with positive charge on the valence band. One hand, the holes transfer to the loaded Pd, and react with the adsorbed H_2O to produce ·OH, which continues to react with CH_4, forming ·CH_3 radicals. On the other hand, the excited electrons react with the adsorbed oxygen to produce ·OOH. Then, the produced ·CH_3 radicals are oxidized to CH_3OH and HCHO by ·OOH, realizing the highly selective CH_4 conversion to high value-added C_1 oxygenates. In this process, the loaded Pd

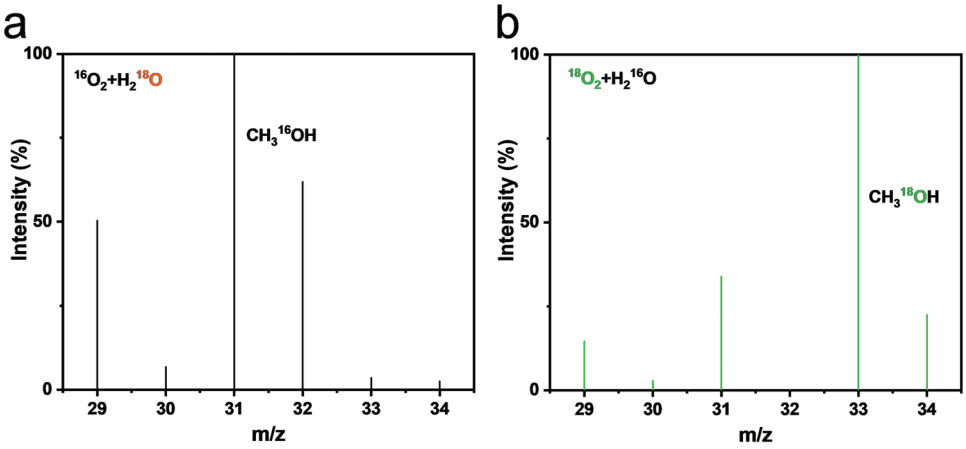

Figure 6. GC-MS spectra of CH_3OH generated over 0.5Pd-ZnTi-LDH-A200 with a) $H_2{}^{18}O + {}^{16}O_2$ or b) $H_2{}^{16}O + {}^{18}O_2$ for CH_4 conversion.

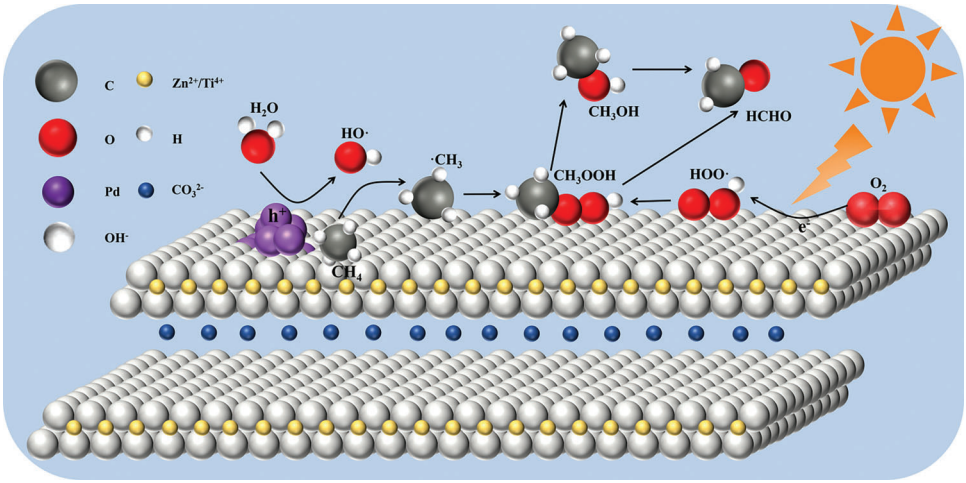

Scheme 1. Proposed photocatalytic mechanism of highly selective oxidation of CH_4 on Pd-ZnTi-LDH-A200.

on the surface of ZnTi-LDH-A200 plays the key roles of CH_4 adsorption sites and hole acceptor, which efficiently increases the chemisorption of CH_4 molecules and promotes the separation of photocarriers in the excited ZnTi-LDH-A200.

3. Conclusion

In summary, the loaded Pd nanoparticles on the 2D-layered ZnTi-LDH-A200 realize highly selective CH_4 conversion to high value-added C_1 oxygenates. The highest production rate achieved is up to be 4924.47 μmol g^{-1} h^{-1} over 0.5Pd-ZnTi-LDH-A200 with the 100% selectivity to C_1 oxygenates, which is 20 times higher than that on the bare ZnTi-LDH-A200. In this reaction, O_2 was demonstrated to be the main oxygen source by isotope labeling experiments. During the photocatalytic process of CH_4 conversion to C_1 oxygenates, the loaded Pd nanoparticles act as the chemisorption sites of CH_4 and the hole acceptor. As the chemisorption site of CH_4, Pd increases the CH_4 adsorption and as the hole acceptor, Pd promotes CH_4 oxidation to $\cdot CH_3$ radicals. Pd furthermore promotes the separation of photocarriers in the excited ZnTi-LDH-A200, facilitating ·OOH production. Two factors result in the significantly enhanced photocatalytic activity of ZnTi-LDH for highly selective CH_4 conversion.

4. Experimental Section

Synthesis of ZnTi-LDH Photocatalysts: ZnTi-LDHs were synthesized using the modified co-precipitation method according to the previous report.[31] The preparation process was as follows: After the dissolution of 1.190 g of $Zn(NO_3)_2{\cdot}6H_2O$ and 0.900 g of urea in 50 mL deionized water, a designed amount of (0.22 mL) of $TiCl_4$ was added dropwise under vigorous stirring for 20 min. Then the mixed solution was transferred to an autoclave and aged at 130 °C for 48 h. The precipitate was centrifuged and washed thoroughly with water and finally dried overnight at 60 °C. At last, 1.0 g sample of the prepared ZnTi-LDH was placed in a porcelain boat and calcined in the muffle furnace at 200 °C for 3 h with a heating rate of 2 °C min^{-1}.[52]

Metal co-Catalysts Loading on ZnTi-LDH: Metal co-catalysts (Au, Ag, Pd, Pt,) were loaded on the surface of ZnTi-LDH photocatalysts by a photo deposition method.[17] Typically, 200 mg photocatalyst was first dispersed into 30 mL methanol by ultrasonication. After being stirred for 5 min, a certain amount of metal precursor ($HAuCl_4$, $AgNO_3$, K_2PdCl_4, H_2PtCl_6) aqueous solution was added into the suspension. By purging with argon for 20 min, the suspension was sealed and irradiated for 3 h at 25 °C under stirring in a multi-channel reactor. Finally, the samples were collected by centrifugation, and washed with methanol and deionized water for three times and dried at 60 °C for 12 h. The as-prepared photocatalysts were denoted as *x*% M-ZnTi-LDH (x = 0.1, 0.3, 0.5, 0.8, and 1.0, which represents the mass percentages of M to ZnTi-LDH; M = Au, Ag, Pd, Pt). As a comparison, M-ZnTi-LDH samples without calcination process were also prepared by the same method above.

Photocatalytic CH_4 Conversion: Direct CH_4 photocatalytic conversion reactions were conducted in a custom-built 200 mL top-irradiation high pressure reactor under full-spectrum irradiation.[44] A Xenon lamp (300 W) (*PLS-SXE300D, Beijing Perfectlight Technology Co., Ltd*) was employed as the light source. The light intensity was measured by the light intensity meter (*PL-MW2000, Beijing Perfectlight Technology Co., Ltd*) and determined to be 150 mW cm^{-2}. In a typical test, 20 mg of the photocatalysts was dispersed uniformly in 100 mL distilled water through ultrasonication. With the gas-tight seal, the suspension was purged with ultrapure O_2 (99.999 vol%) for 20 min to completely remove air. Then, 0.1 MPa O_2 was maintained in the reactor. Next, CH_4 (99.999 vol%) was injected to acquire the desired pressure (1.9 MPa). The reaction was conducted for 2 h at 25 °C with a circulating cooling system. Gaseous products as well as CH_3OH in liquid products were measured by the gas chromatograph (*GC-2014, Shimadzu Co., Ltd*) equipped with a thermal conductivity detector (TCD) and a flame ionization detector (FID).[33] Formaldehyde (HCHO) was quantified through the colorimetric method[48] on the UV–vis absorbance spectrometer (*UV-3600 Plus, Shimadzu Co., Ltd*). CH_3OOH and CH_3OH were also analyzed by the nuclear magnetic resonance (NMR) spectra of ^1H and ^{13}C via an NMR equipment (*AVANCE III JEOL Ltd*).

Cyclic experiments were also carried out to investigate the stability of the optimal photocatalyst. The used photocatalysts were centrifuged to collect after the reaction, then washed with deionized water, dried in the oven at 60 °C, and calcined at 200 °C for 3 h to remove the surface adsorbed carbides.

Isotope Labeling Experiment: To explore the source of carbon in the products, 20 mg of the photocatalyst was dispersed in 3 mL H_2O and degassed for 30 min to completely remove air. The reactor was then refilled with 0.5 MPa $^{13}CH_4$ (99 vol%) or 0.5 MPa $^{12}CH_4$ and 0.1 MPa O_2 (99.999 vol%), respectively. The reaction was also carried out at 25 °C for 6 h. The products were measured by ^{13}C NMR (*AVANCE III JEOL Ltd*).

For oxygen source investigation: 20 mg of the photocatalysts was dispersed in 3 mL $H_2{}^{16}O$ or $H_2{}^{18}O$ (99%), respectively. The reactor was

then degassed for 30 min to completely remove air, prior to being refilled with 1.9 MPa CH_4 (99.999 vol%) and 0.1 MPa $^{18}O_2$ (98%) or $^{16}O_2$ (99.999 vol%). The reaction was carried out at 25 °C for 6 h. The products were measured by GC-MS (*QP2020, Shimadzu Co., Ltd*) that equipped with Cap WAX column.

Monitor of Hydroxyl Radicals (·OH) and Hydroperoxyl Radicals (·OOH): In situ electron paramagnetic resonance (EPR) was used to monitor the generation of ·OH and ·OOH radicals before and after light irradiation.[56,60] For the detection of ·OH radicals, 10 mg of the photocatalysts was suspended in 5 mL water, with DMPO as the trapping agent. For detecting ·OOH radicals, 10 mg catalyst was suspended in 5 mL acetonitrile, with DMPO as the trapping agent as well.

Nitrotetrazolium blue chloride (NBT) was used as the probe molecule to measure the generation of $O_2^{-\cdot}$ radicals.[59] Typically, 10 mg of the photocatalysts was mixed with 100 mL NBT solution (0.02 mM) and stirred in dark for 15 min. After light irradiation, a certain amount of the reactants was sampled at every 10 min intervals. UV–vis spectra were then detected on *UV-3600 Plus* spectrofluorometer after being filtered.

The photoluminescence (PL) technique was used to test the ·OH generation because of the reaction between ·OH and coumarin (CA) to generate 7-hydroxycoumain (7-OH-CA), which could be detected by photoluminescence spectra at 450 nm.[61] Typically, 10 mg of the photocatalysts was dispersed in 100 mL CA aqueous solution (0.5 mM) and stirred in dark for 15 min. The light was turned on, then the suspension was filtered and sampled at every 10 min intervals. At last, the generation of 7-OH-CA was measured by *F-4500* spectrofluorometer.

Supporting Information

Supporting Information is available from the Wiley Online Library or from the author.

Acknowledgements

All authors are grateful for the Shaanxi Key Research Grant (China, 2020GY-244). H.-Y. Jiang is grateful for the financial supports of Basic research program of Nature Science in Shaanxi Province (No. 2021JQ-442).

Conflict of Interest

The authors declare no conflict of interest.

Data Availability Statement

The data that support the findings of this study are available from the corresponding author upon reasonable request.

Keywords

C_1 products, methane conversion, Pd co-catalysts, photocatalysis, ZnTi-LDH

Received: April 14, 2023
Revised: June 2, 2023
Published online:

[1] H. Song, X. Meng, Z. Wang, H. Liu, J. Ye, *Joule* **2019**, *3*, 1606.
[2] H. Jahangiri, J. Bennett, P. Mahjoubi, K. Wilson, S. Gu, *Catal. Sci. Technol.* **2014**, *4*, 2210.
[3] J.-M. Lavoie, *Front. Chem.* **2014**, *2*, 81.
[4] X. Li, C. Wang, J. Tang, *Nat. Rev. Mater.* **2022**, *7*, 617.
[5] P. Schwach, X. Pan, X. Bao, *Chem. Rev.* **2017**, *117*, 8497.
[6] M. Mohamedali, O. Ayodele, H. Ibrahim, *Renewable Sustainable Energy Rev.* **2020**, *131*, 110024.
[7] N. Agarwal, S. J. Freakley, R. U. McVicker, S. M. Althahban, N. Dimitratos, Q. He, D. J. Morgan, R. L. Jenkins, D. J. Willock, S. H. Taylor, C. J. Kiely, G. J. Hutchings, *Science* **2017**, *358*, 223.
[8] J. Zhao, X. Guo, R. Shi, G. I. N. Waterhouse, X. Zhang, Q. Dai, T. Zhang, *Adv. Funct. Mater.* **2022**, *32*, 2204056.
[9] Z. Zhu, W. Guo, Y. Zhang, C. Pan, J. Xu, Y. Zhu, Y. Lou, *Carbon Energy* **2021**, *3*, 519.
[10] Q. Li, Y. Ouyang, H. Li, L. Wang, J. Zeng, *Angew. Chem., Int. Ed.* **2022**, *61*, e202108069.
[11] S. Bai, Q. Yao, Y. Xu, K. Cao, X. Huang, *Nano Energy* **2020**, *71*, 104566.
[12] K. Zheng, Y. Wu, Z. Hu, X. Jiao, L. Li, Y. Zhao, S. Wang, S. Zhu, W. Liu, W. Yan, Y. Sun, Y. Xie, *Nano Lett.* **2021**, *21*, 10368.
[13] L. Luo, J. Luo, H. Li, F. Ren, Y. Zhang, A. Liu, W.-X. Li, J. Zeng, *Nat Commun.* **2021**, *12*, 1218.
[14] S. Song, H. Song, L. Li, S. Wang, W. Chu, K. Peng, X. Meng, Q. Wang, B. Deng, Q. Liu, Z. Wang, Y. Weng, H. Hu, H. Lin, T. Kako, J. Ye, *Nat. Catal.* **2021**, *4*, 1032.
[15] N. Feng, H. Lin, H. Song, L. Yang, D. Tang, F. Deng, J. Ye, *Nat Commun.* **2021**, *12*, 4652.
[16] H. M. T. Galvis, K. P. de Jong, *ACS Catal.* **2013**, *3*, 2130.
[17] A. Tanaka, K. Hashimoto, H. Kominami, *J. Am. Chem. Soc.* **2012**, *134*, 14526.
[18] M. Ravi, M. Ranocchiari, J. A. van Bokhoven, *Angew. Chem., Int. Ed.* **2017**, *56*, 16464.
[19] G. Fan, F. Li, D. G. Evans, X. Duan, *Chem. Soc. Rev.* **2014**, *43*, 7040.
[20] S.-J. Xia, F.-X. Liu, Z.-M. Ni, W. Shi, J.-L. Xue, P.-P. Qian, *Appl. Catal. B* **2014**, *144*, 570.
[21] S.-M. Xu, H. Yan, M. Wei, *J. Phys. Chem. C* **2017**, *121*, 2683.
[22] G. Mishra, B. Dash, S. Pandey, *Appl. Clay Sci.* **2018**, *153*, 172.
[23] M. Xu, M. Wei, *Adv. Funct. Mater.* **2018**, *28*, 1802943.
[24] Y. Zhao, G. Chen, T. Bian, C. Zhou, G. I. N. Waterhouse, L.-Z. Wu, C.-H. Tung, L. J. Smith, D. O'Hare, T. Zhang, *Adv. Mater.* **2015**, *27*, 7824.
[25] C. Li, M. Wei, D. G. Evans, X. Duan, *Small* **2014**, *10*, 4469.
[26] G. Cui, X. Meng, X. Zhang, W. Wang, S. Xu, Y. Ye, K. Tang, W. Wang, J. Zhu, M. Wei, D. G. Evans, X. Duan, *Appl. Catal. B* **2019**, *248*, 394.
[27] X. Xiong, Y. Zhao, R. Shi, W. Yin, Y. Zhao, G. I. N. Waterhouse, T. Zhang, *Sci. Bull.* **2020**, *65*, 987.
[28] H. Jiang, K.-i. Katsumata, J. Hong, A. Yamaguchi, K. Nakata, C. Terashima, N. Matsushita, M. Miyauchi, A. Fujishima, *Appl. Catal. B* **2018**, *224*, 783.
[29] K. Yan, G. Wu, W. Jin, *Energy Technol.* **2016**, *4*, 354.
[30] Y. Zhao, L. Zheng, R. Shi, S. Zhang, X. Bian, F. Wu, X. Cao, G. I. N. Waterhouse, T. Zhang, *Adv. Energy Mater.* **2020**, *10*, 2002199.
[31] M. Shao, J. Han, M. Wei, D. G. Evans, X. Duan, *Chem. Eng. J.* **2011**, *168*, 519.
[32] J. Wang, L. Zhao, H. Shi, J. He, *Angew. Chem., Int. Ed.* **2011**, *50*, 9171.
[33] L. Luo, Z. Gong, Y. Xu, J. Ma, H. Liu, J. Xing, J. Tang, *J. Am. Chem. Soc.* **2022**, *144*, 740.
[34] H. Song, X. Meng, S. Wang, W. Zhou, S. Song, T. Kako, J. Ye, *ACS Catal.* **2020**, *10*, 14318.
[35] J. Xie, R. Jin, A. Li, Y. Bi, Q. Ruan, Y. Deng, Y. Zhang, S. Yao, G. Sankar, D. Ma, J. Tang, *Nat. Catal.* **2018**, *1*, 889.
[36] A. Grzegórska, I. Wysocka, P. Głuchowski, J. Ryl, J. Karczewski, A. Zielińska-Jurek, *Chemosphere* **2022**, *308*, 136191.
[37] M. Kruk, M. Jaroniec, *Chem. Mater.* **2001**, *13*, 3169.
[38] K. Jing, Y. Fu, Z. Chen, T. Zhang, J. Sun, Z. Xu, G. Guo, *ACS Appl. Mater. Interfaces* **2021**, *13*, 24856.

[39] J. Zou, Z. Wang, W. Guo, B. Guo, Y. Yu, L. Wu, *Appl. Catal. B* **2020**, *260*, 118185.
[40] Y. Zhu, R. Zhu, G. Zhu, M. Wang, Y. Chen, J. Zhu, Y. Xi, H. He, *Appl. Surf. Sci.* **2018**, *433*, 458.
[41] Z. Sheng, F. Hou, L. Zou, Y. Li, J. Li, J. Li, L. Ai, W. Wei, A. Wei, *J. Photochem. Photobiol.* **2022**, *432*, 114114.
[42] J. Li, Y. Xu, Z. Ding, A. H. Mahadi, Y. Zhao, Y.-F. Song, *Chem. Eng. J.* **2020**, *388*, 124248.
[43] Y. Liao, J. Qian, G. Xie, Q. Han, W. Dang, Y. Wang, L. Lv, S. Zhao, L. Luo, W. Zhang, H.-Y. Jiang, J. Tang, *Appl. Catal. B* **2020**, *273*, 119054.
[44] H. Song, X. Meng, S. Wang, W. Zhou, X. Wang, T. Kako, J. Ye, *J. Am. Chem. Soc.* **2019**, *141*, 20507.
[45] L. Luo, L. Fu, H. Liu, Y. Xu, J. Xing, C.-R. Chang, D.-Y. Yang, J. Tang, *Nat. Commun.* **2022**, *13*, 2930.
[46] Y. Fan, W. Zhou, X. Qiu, H. Li, Y. Jiang, Z. Sun, D. Han, L. Niu, Z. Tang, *Nat. Sustain.* **2021**, *4*, 509.
[47] W. Zhou, X. Qiu, Y. Jiang, Y. Fan, S. Wei, D. Han, L. Niu, Z. Tang, *J. Mater. Chem. A* **2020**, *8*, 13277.
[48] J. Chen, S. Stepanovic, A. Draksharapu, M. Gruden, W. R. Browne, *Angew. Chem., Int. Ed.* **2018**, *57*, 3207.
[49] Z. Gong, L. Luo, C. Wang, J. Tang, *Solar RRL.* **2022**, *6*, 2200335.
[50] Q.-Q. Yan, D.-X. Wu, S.-Q. Chu, Z.-Q. Chen, Y. Lin, M.-X. Chen, J. Zhang, X.-J. Wu, H.-W. Liang, *Nat. Commun.* **2019**, *10*, 4977.
[51] J. M. Watson, U. S. Ozkan, *J. Catal.* **2002**, *210*, 295.
[52] Y. Xu, X. Sun, X. Wang, L. He, M. T. Wharmby, X. Hua, Y. Zhao, Y. Song, *Chemistry* **2021**, *27*, 13211.
[53] C. D. Wagner, *Handbook of X-Ray Photoelectron Spectroscopy*, Perkin-Elmer, Waltham, USA **1979**.
[54] S. M. Prokes, J. L. Gole, X. Chen, C. Burda, W. E. Carlos, *Adv. Funct. Mater.* **2005**, *15*, 161.
[55] Y. Nakaoka, Y. Nosaka, *J. Photochem. Photobiol.* **1997**, *110*, 299.
[56] Y. Nosaka, A. Y. Nosaka, *Chem. Rev.* **2017**, *117*, 11302.
[57] Y.-R. Hong, S. Dutta, S. W. Jang, O. F. Ngome Okello, H. Im, S.-Y. Choi, J. W. Han, I. S. Lee, *J. Am. Chem. Soc.* **2022**, *144*, 9033.
[58] M. Hayyan, M. A. Hashim, I. M. AlNashef, *Chem. Rev.* **2016**, *116*, 3029.
[59] X. Ran, L. Duan, X. Chen, X. Yang, *J. Mater. Sci.* **2018**, *53*, 7048.
[60] H. Hou, X. Zeng, X. Zhang, *Angew. Chem., Int. Ed.* **2020**, *59*, 17356.
[61] A. C. Maier, E. H. Iglebaek, M. Jonsson, *ChemCatChem* **2019**, *11*, 5435.
[62] P. Wang, R. Shi, Y. Zhao, Z. Li, J. Zhao, J. Zhao, G. I. N. Waterhouse, L.-Z. Wu, T. Zhang, *Angew. Chem., Int. Ed.* **2023**, *62*, e202304301.